W. Gleissle[1] and J. Curry[2]

[1] Institut für Mechanische Verfahrenstechnik und Mechanik, Universität Karlsruhe, Karlsruhe, Germany
[2] Coperion Werner & Pfleiderer, Ramsey, N. J., USA

Characterisation of Finite Length Composites

Rheological Studies of Processed PP-Glass Composites

In cooperation with: H. M. Laun, BASF-Aktiengesellschaft, J. Lawler Celanese USA, R. Bailey, ICI, Wilton UK, M. Lecomte, Shell Research and Techn. Center, Louvain-la-Neuve, C. Dehennau, Solvay, Brussels, W. Gleissle, Universität Karlsruhe, J. Curry, Coperion Werner & Pfleiderer, USA

This paper is a technical report about the structure and the rheological behaviour of processed polypropylene-glass fibre composites. The present studies has been carried out as a part of the international project on the Characterization of Finite Length Composites initiated and organized by the IUPAC Working Party: Structure and Properties of Commercial Polymers. Seven industrial and university laboratories in Europe and in USA worked together in a common project to investigate the influence of the processing conditions on the rheology and manufacturing behaviour of polymer-glass composites preprocessed in a twin screw extruder. All investigations presented concern the influence of the processing procedure on the structure of the composites such as fiber length destribution, fiber orientation, destribution of the fibre concentration in the sample and the rheology of the composites. The flow behaviour dependent on the processing conditions has been measured using capillary rheometers to investigate the viscosity functions, the entrance and outlet pressures losses as well as for observations of the shape and internal structure of extruded composites. Torsional rheometers for low shear rate, oscillatory and transient viscosity behaviour and for the quantification of fibre orientation with ongoing shear process. Additionaly queeze flow experiments are made.

Most laboratories used analogous recording sytems to documente the primary experimental results. So results are partially given here as direct copies from the original data readings. The different data handling and the transfer of data from laboratory to laboratory for comparison of results leads sometimes to unavoidable inhomogeneous (due to the style and possibilities of the different laboratories) presentation of the results. The present report is a result of data collecting, data comparison and documentation of results over a period of nearly ten years.

* Mail address: W. Gleissle, Inst. f. Mech. Verfahrenstechnik und Mechanik, Universität Karlsruhe

1 Processing Procedure (Fig. 1)

The purpose of the reprocessing procedure was to prepare pelletized and strip product with sequentially degraded fibre length. The virgin material is the commercial product, M-Verton, a pultruded polypropylene composite containing 10 mm glass fiber at 40 % loading (wt) in strand cut pellets. In preceeding reports, the code for this material has been PP/g10.

The reprocessing procedure (done by Werner & Pfleiderer, USA), was the successive processing through a plasticating corotating compounding extruder and extrusion alternately through a strip and a pellet die. Extrusion temperature was

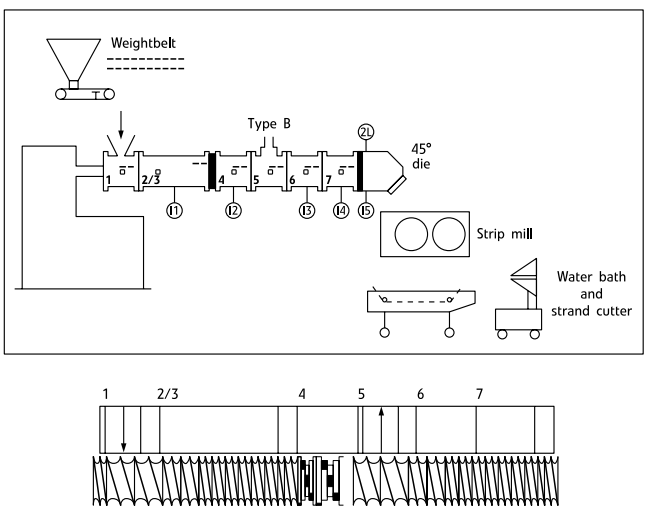

Fig. 1. Flow Diagram and screw design for pellet reprocessing

A) B) C)

Fig. 2. Glass fibre length of PP/g 10 feed stock (A) and after first (B) and second (C) reprocessing cycle

200 °C. A screw configuration appropriate for plastication of polypropylenen has been installed. In a first step strips (B/H = 20.5/3 mm, code 1S) and pellets (L/D = 10/2.5, code 1P) were produced. The extrusion pressure p has been 30 bar to extrude strips and 71 bar (with significant pressure fluctuations) for pellets.

In a second step pellets (1P) have been recycled as feedstock to produce strips (sample 2S) and pellets (sample 2P) with the same twinscrew configuration. A strong reduction of the extrusion pressure from 30 to 5 bar for strips and from 71 to 10 bar for pellets has been observed, documenting the remarkable change of processing properties due to the first processing step.

2 Material Characterization – Fibre Length Reduction

2.1 Average Fibre Length and Fibre Length Distribution

The general structural effects of reprocessing are reduction of fibre length, improved glass-matrix adhesion, and increasingly random fiber orientation.

Photomicrographs of ashed fibres show progressive reduction of the fibre length with subsequent processing, Fig. 2.

Sample	Fibre length/mm	Lab.	Comment
1S	2.461	ICI, Wilton, UK	Long, multimodal distribution
1P	1.16	ICI, Wilton, UK	Long, multimodal distribution
1P	0.69	Shell Research and Tech. Center, Louvain la Neuve	
2S	0.71	ICI, Wilton, UK	Short, narrow distribution
2P	0.64	ICI, Wilton, UK	Short uniform fibre
2P	0.46	Shell Research and Tech. Center, Louvain la Neuve	

Table 1. Average fibre length after reprocessing

Strip and pellet samples produce nearly the same glass fibre length distribution.

As shown in principle the processing of the virgin material PP/g10 leads to a pronounced reduction of the originally uniform fibre length. Fibre length measurements have been carried out at ICI, Wilton, UK (Seescan Solitaire Systeme, counting 600 fibres burned out at 550 °C) and Shell Research and Tech. Center, Louvain la Neuve (PC-Scope, image analysis, Automation and Robotics, 500 fibres analized burned out at 500 °C). The use of different methods results in different average fibre length (Table 1).

One reason for this discrepancy are the different analyzing systems and different operators on the one hand but secondly the samples histories are different. ICI, Wilton, UK sampled the reprocessed material as delivered. Shell Research and Tech. Center, Louvain la Neuve sampled the discharge of a capillary rheometer test of the delivered material. The breadth of the fi-

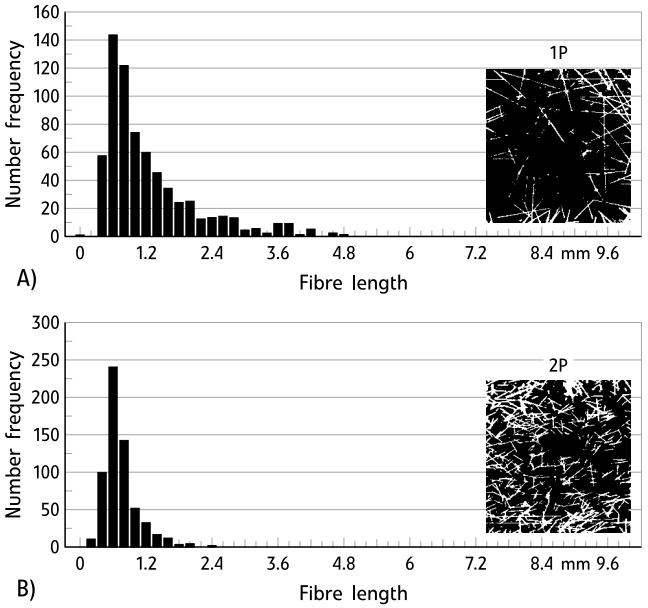

Fig. 3. Fibre length distributions after reprocessing: 1 P (one cycle), 2 P (two cycles); 600 fibre population

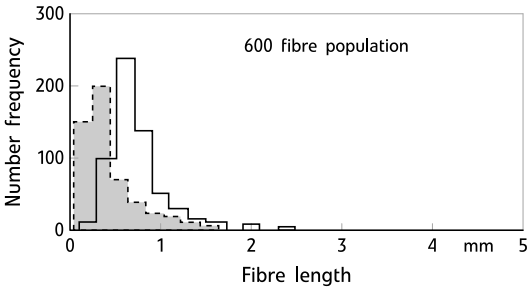

Fig. 4. Fibre length distribution of sample 2 P before, (–), and after capillary measurements, (- - -)

bre length distributions is the same in both laboratories but the rheometer tested sample has a shorter average fiber length (Fig. 3).

This shift of the fibre length distribution to shorter fiber length may be caused by the capillary viscosity measurement itself and can be seen in Fig. 4. This result demonstrates first that the capillary rheometer simulates an (injection-) molding process and second, that the measuring procedure itself changes the material structure.

The real fibre content of about 43 % found by the Shell Research and Tech. Center, Louvain la Neuve and Werner & Pfleiderer, USA is slightly higher than the nominal content of 40 %.

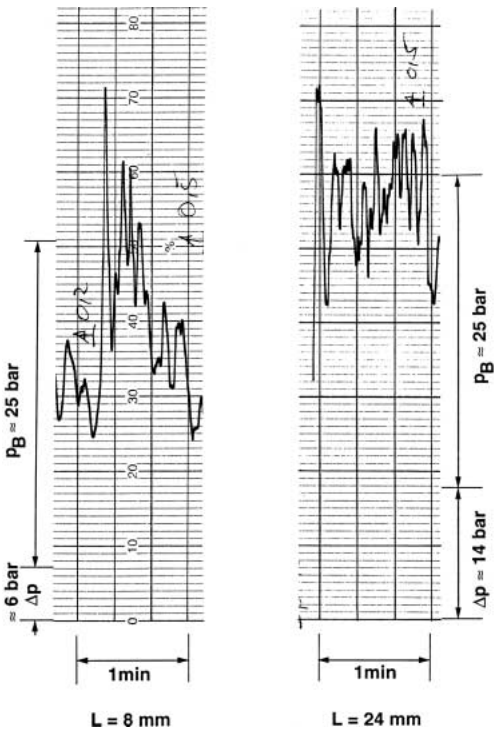

Fig. 5. Readings of extrusion pressure of virgin Verton PP/g10 material for different capillary lengths L but equal extrusion velocity, p_B = Bagley pressure, Δp = pure viscous pressure drop, capillary diameter d = 2.1 mm, extrusion velocity v = 25.5 mm/s, apparent shear rate D = 97.2 s^{-1}, T = 200 °C

3 Flow Behaviour

3.1 Capillary Flow – Slit- and Round Bore Capillaries

3.1.1 Pressure Scattering

The flow properties of virgin feed material Verton PP/g10 and PP/g5 are mentioned in the introductory papers from *Cervenka* and *Allen* [1], *v. Bradsky* et al. [2] and are documented in detail in the paper of *Bailey* and *Groves* [3].

The general result of the current work is a strongly fluctuating extrusion pressure at slit and round bore capillary flow. As a consequence the viscosity functions $\eta(\dot{\gamma})$ show broad scattering especialy at low shear rates. Unusually high entrance pressure losses (Bagley pressures p_B) are interpreted as a pronounced elongational viscosity of both materials. As an example of the entry pressure effect, pressure readings for the extrusion of PP/g10 through capillaries of different length but same diameter at constant extrusion rate are given in Fig. 5. The pressure drop over the short die (L = 8 mm) is nearly as high as over the three times longer die (L = 24 mm).

The scattering of the extrusion pressure is strongly reduced after the sample has passed the first reprocessing cycle. The average pressure is much lower and the pure viscous pressure drop becomes more significant, resulting in a stronger influence of the capillary length on the total pressure drop, as can be seen in Fig. 6A. The pressure readings after the second reprocessing cycle at the same extrusion conditions are shown in Fig. 6B. They are again lower, more regular and more strongly affected by capillary length.

The processing conditions change the flow properties and hence the injection molding behaviour in a pronounced manner. The pressure readings of samples PP/g10 (virgin material, precursor) and 1S and 2S can immediately be compared in Fig. 7. At the same extrusion conditions one finds a strongly reduced total pressure drop from about 43 bar (average) to 17.5 bar.

3.1.2 Bagley-Correction Pressure

Calculating the flow functions from the raw datas one finds a strongly decreasing viscosity function from one reprocessing cycle to the other. The apparent viscosity $\eta_a(D)$ calculated from the total pressure drop using a 8 mm capillary of 2.1 mm diameter for the Verton PP/g10 and the processed material 1P and 2P are shown in Fig. 8.

After two reprocessing cycles the apparent viscosity function, measured with a short die, is in average 7 times lower as for the virgin composite. The tremendous reduction of the apparent viscosity (for short dies) is mainly caused by the reduction of the entrance and outlet pressure, collectively called Bagley(-correction) pressure. The intersection of the linear extrapolation of the measured pressure plotted over the capillary length L at L = 0 (Bagley-correction) is reduced from p_B = 85 bar to 12 bar for successive reprocessing as shown in Fig. 9. The slope of the straight lines, describing the flow resistance inside the capillary, is not influenced significantly by the reprocessing (as can be taken from the linearized pressure drop equations in Fig. 9). Hence, the true (Bagley corrected) viscos-

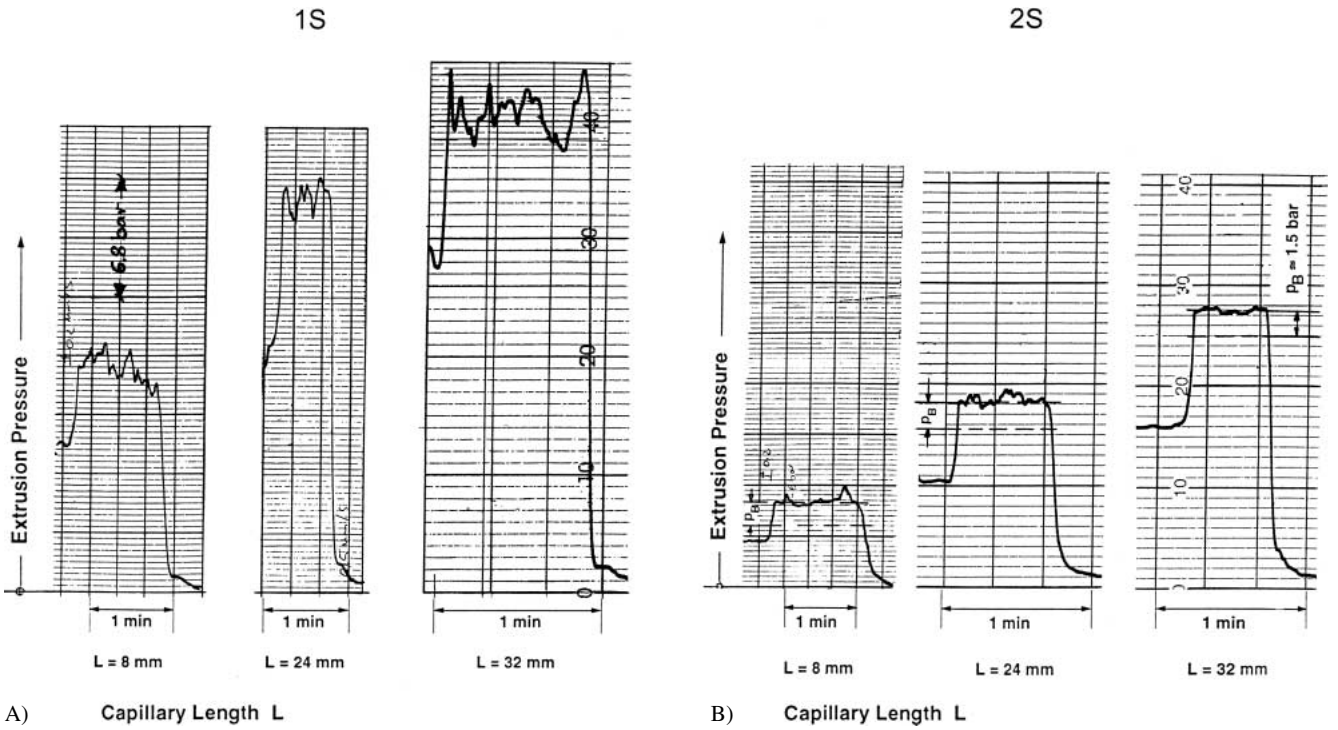

Fig. 6. Extrusion pressures after one (A) and two (B) reprocessing cycles at the same extrusion velocity but different capillary lengths L, extrusion conditions see Fig. 5

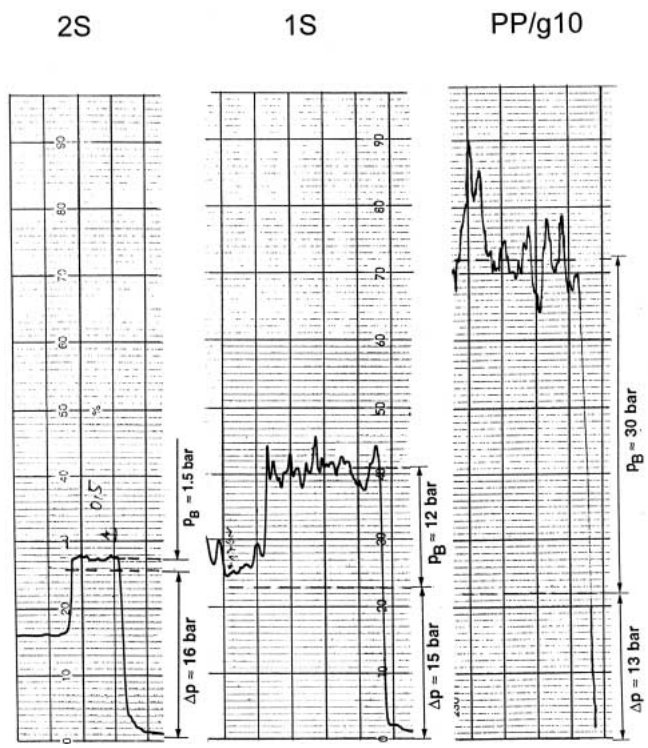

Fig. 7. Pressure readings for samples PP/g10 and the reprocessed samples 1 S and 2 S at the same extrusion conditions (see Fig. 5), L = 32 mm

ity seems not to be influenced significantly by the fibre length reduction.

The Bagley-correction pressure is the flow property which is mostly reduced by the reprocessing of the composite. The main reason for that change is the reduction of entrance resistance of the composite into the capillary.The reduction of about a factor of 7 after two cycles is the same as the apparent viscosity reduction. In other words, the change of the apparent viscosity is mainly effected by the reduction of p_B with the processing cycles resp. fibre length (compare *Laun* [4]). This is documented in Fig. 10.

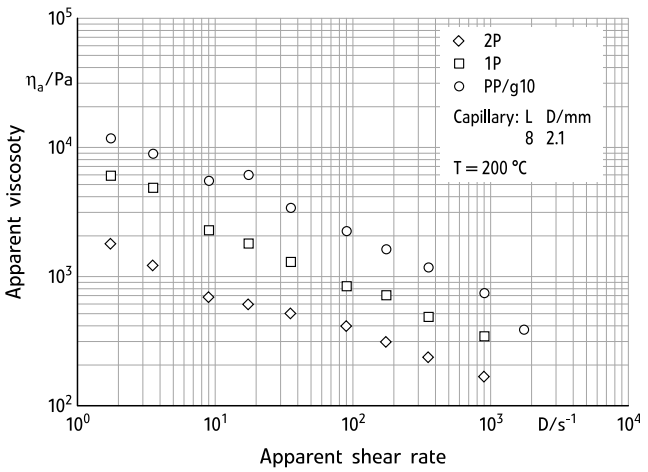

Fig. 8. Apparent viscosity functions $\eta_a(D)$ of the virgin material PP/g10 and the reprocessed materials 1 P and 2 P

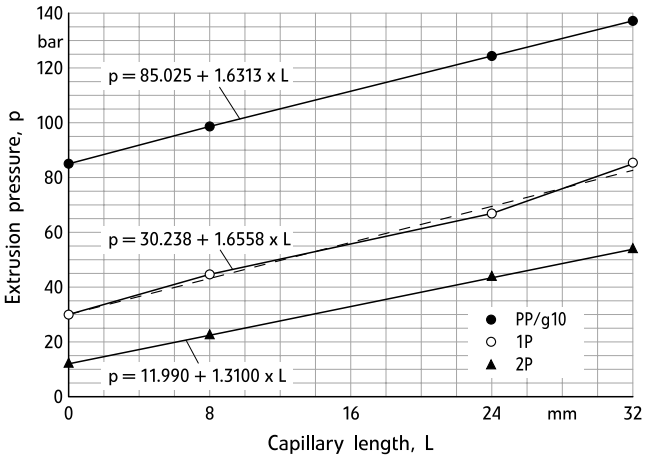

Fig. 9. Pressure drop p as a function of the capillary length L ("Bagley-Plot") of virgin material PP/g10 and the reprocessed samples 1P and 2P, D = 970 s^{-1}, T = 200 °C

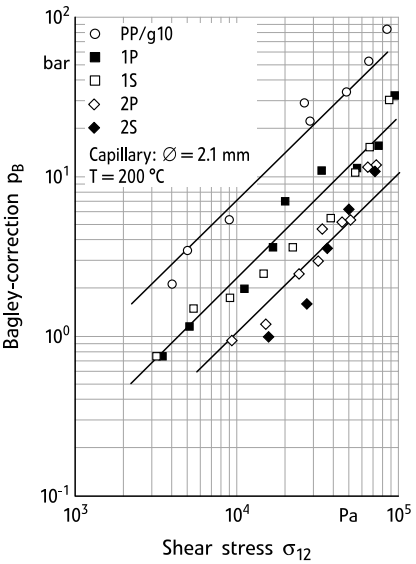

Fig. 10. Bagley-correction pressure of the virgine material PP/g10 and the reprocessed samples 1P and 2P as a function of the shear stress σ_{12}

The scattering of the data is due to the normal scattering of results investigated from different laboratories.

In consequence the true viscosity $\eta(\dot{\gamma})$ (describing the pure flow resistance inside a capillary, see Fig. 11), calculated from the Bagley corrected shear stresses σ_{12} according Eqs. 1 and 2 is not significantly effected by the processing.

$$\sigma_{12} = (p - p_B)/(4L/D_D), \quad (1)$$

$$\eta(\dot{\gamma}) = \tau(\dot{\gamma})/\dot{\gamma}. \quad (2)$$

The corrected viscosity function for all samples (virgin and processed material Fig. 11) show significant scattering especially at low shear rates. There seems to be a decrease of the viscosity with ongoing processing, but a definite quantification is not possible. The full line in Fig. 11 represents the viscosity function of the clear PP-matrix fluid. The dashed line is the reduced viscosity ηB of the matrix as a function of the reduced shear rate $\dot{\gamma}/B$. This curve results from the shift of the matrix polymer viscosity function $\eta(D)$ according the concept of the shear stress equivalent intrinsic shear rate (*Gleissle* and *Baloch* [5], *Ohl* and *Gleissle* [6]) with the experimentaly determined shift factor B = 3.5. This dashed curve agrees with the average viscosity function of the composite materials (before and after processing). The flow behaviour of the composite is dominated by the viscosity function of the clear matrix.

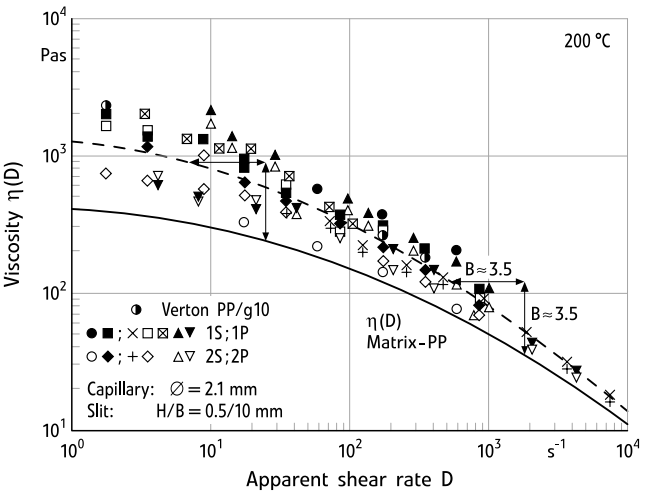

Fig. 11. Bagley corrected viscosity functions of PP/g10 and the reprocessed samples 1P and 2P

3.1.3 Some Remarks on the Influence of the Capillary Entry Angle

Clear matrix polymer PP, Virgin pultruded Verton PP/g10, PP/g5 injection molding material, and the reprocessed materials 1P and 2P were tested in capillary rheometers with short capillaries L/R = 1. Different entry angles (total) $10° < \alpha < 135°$ were applied to investigate the elongation flow behaviour of the composites before entering the capillary. Independent of the of the entrance angle the pressure transducer was positioned at the same distance to the entrance of the capillary, Solvay, Brussels.

For the clear matrix polymer an increasing entry pressure drop with decreasing cone angle was found. (see *Bailey* and *Groves* [3]). This increasing pressure drop with decreasing cone angle seams to be dominated by viscous effects. All fibre composites, virgin and reprocessed materials, on the other hand exhibit a slightly decreasing pressure drop with decreasing entry cone angle, which may be effected by improved orientation of the fibres in a more slender entrance region.

3.1.4 Distribution of Fibre Content in the Extrudate

To study the effect of the capillary experiment itself on the fibre length distribution and on the fibre content, samples were analyzed at the beginning and end of a capillary experiment, Shell Research and Tech. Center, Louvain la Neuve. When the

Composite	#	Beg. of exp.	End of exp.	Die entrance
1P	1	44.2	39.7	–
	2	42.8	37.2	42.5
	Average	43.5	38.4	42.5
2P	3	42.4	41.9	43.1
	4	41.9	42.3	43.2
	Average	42.2	42.1	43.1

Table 2. Fibre content after first and second ram (% wt)

Composite	#	Beg. of exp.	End of exp.	Die entrance
1P	1	0.66	0.80	–
	2	0.50	0.77	0.71
	Average	0.58	0.78	0.71
2P	3	0.31	0.41	0.56
	4	0.42	0.43	0.62
	Average	0.37	0.42	0.59

Table 3. Average fibre length after first and second pass through the capillary

experiment was stopped, material remaining in the die entrance was analyzed In each case measurements were repeated. (#1 and 2 on sample 1P and #3 and 4 on 2P).

From the results, given in Table 2, one gets the impression that the die gradually acts as a filter (especialy for 2P) so that fibres are assembled near the die entrance. The average fibre content was found to be slightly above 40 %. Measurement of the fibre content in the reprocessed samples 1P, 1S and 2P and 2S at Werner & Pfleiderer, USA immediately after processing in the ZSK give the same fibre content of about 43 % by weight as was found at Shell Research and Tech. Center, Louvain la Neuve.

In the light of Table 3, it is clear, that the effect of an additional ram extrusion is to initially reduce the fibre length. The average fibre length in the extrudate increased during the experiment. There is a preferred accumulation of long fibres near the die entrance.

The original pressure readings (Fig. 12) from a Rosand twin capillary rheometer with two parallel mounted dies (one long and one short) with the same diameter, document, that for the same apparent shear rate, the same pressure was found at the beginning and end of the experiment. That means, that the slight accumulation of fibres near the entrance do not influence the rheometric measurements.

The investigation of the flow functions of long fibre composites by means of capillary rheometry illustrates the dramatic change of processing properties (especially injection molding behaviour) caused by reprocessing the composites. While the capillary entrance pressure (Bagley-correction) losses are sharply reduced by the fibre length reduction, the steady state corrected viscosity is less influenced. In practice it follows that preprocessing influences the injection molding conditions especially for complex shaped forming tools.

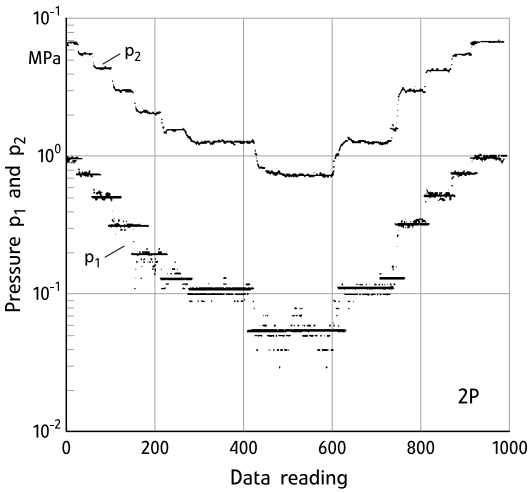

Fig. 12. Long and short die pressure values (apparent shear rates from 768 to 19.2 to 768 s^{-1})

3.2 Torsional Flow: Parallel Plate and Cone and Plate Rheometer

3.2.1 Complex and Steady State Viscosity Functions

Complex viscosity η* and transient viscosity η(t) of the reprocessed materials 1P and 2P has been investigated in Shell Research and Tech. Center, Louvain la Neuve. Dynamic parallel plate rheometer experiments on plates with d = 50 mm diameter and plate separation H = 2.2 mm have been carried out. The oscillation frequency was varied in the range $1 < \omega < 500\ s^{-1}$ at T = 200 °C.

The output wave form of the torque was found to be pure sinusoidal and, as demonstrated in Fig. 13, the complex viscosity is strongly dependent on the strain. Linear viscoelastic behaviour is found approximately only at very small shear strains $\gamma < 0.1$ %. At greater strains, the complex viscosity of either sample is strongly decreasing with increasing strain for both frequencies.

Modified Casson plots *(L. Utracky* [7]) have been calculated to determine yield stress effects. The extrapolation of these functions to vanishing low frequencies suggest the presence of

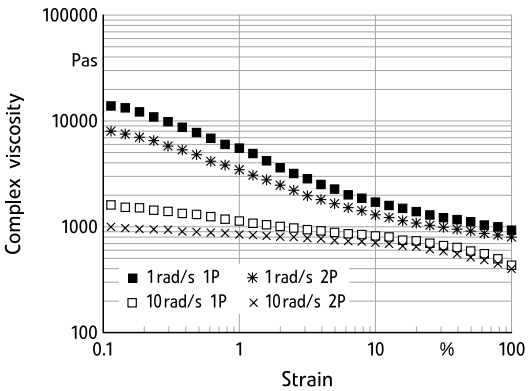

Fig. 13. Complex viscosity η^* of samples 1P and 2P at different frequencies ω = 1 and 10 s^{-1} as a function of the shear strain

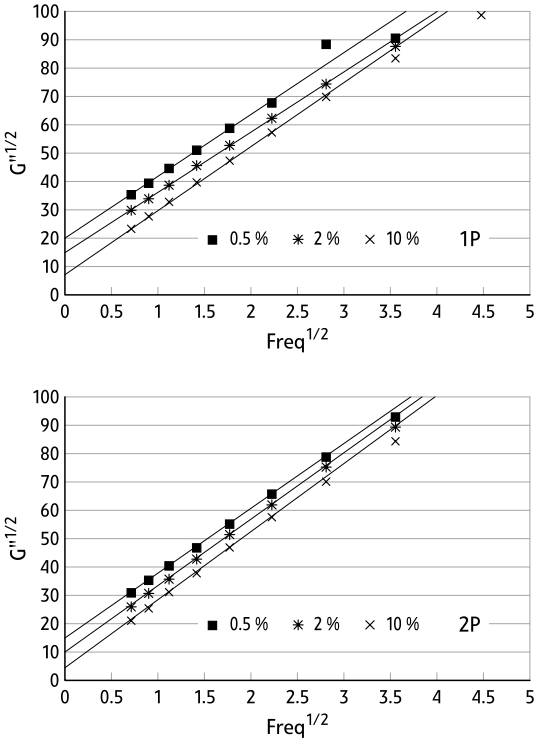

Fig. 14. Modified Casson plots of the reprocessed composites 1P and 2P

an apparent yield modulus, Fig. 14. There is fairly close aggreement for smaller strain to produce higher yield values. Compared at the same strain, the apparent yield values of the twice reprocessed material seem to be lower than the values of single reprocessed material.

Comparison of parallel plate and capillary rheometer results, Fig. 15, show the typical result: At low frequencies and shear rates and very small strains the Cox-Merz rule, Eq. 3, may be more or less fairly satisfied, at higher frequencies and shear rates the complex viscosity $\eta^*(\omega)$ is much higher than the shear viscosity $\eta(D)$.

$$\eta^*(\omega) = \eta(D),\ D = \omega. \qquad (3)$$

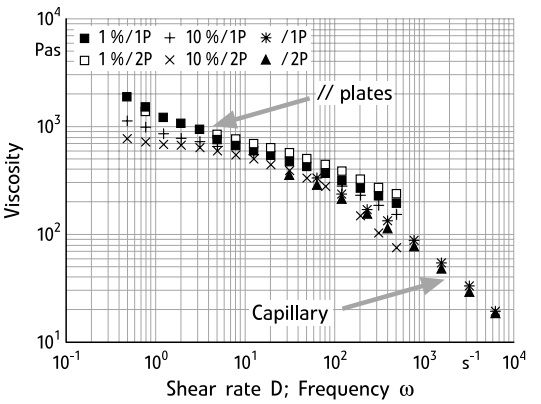

Fig. 15. Complex viscosity $\eta^*(\omega)$ at different strains and the shear viscosity $\eta(D)$ of the reprocessed composites 1P and 2P

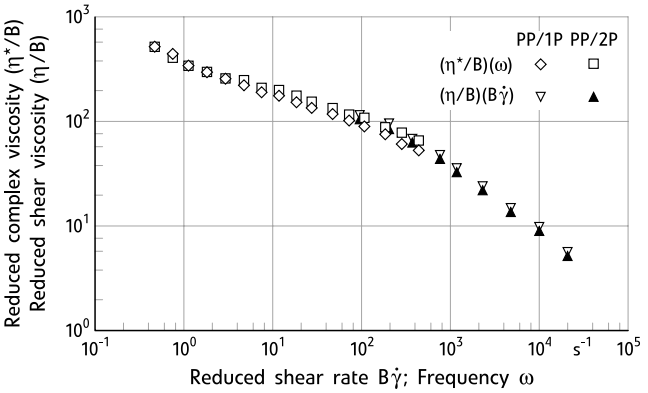

Fig. 16. Reduced complex viscosity and shear viscosity functions of samples 1P and 2P (applied strain γ = 1 %)

Applying the concept of shear stress equivalent shear rate (*Gleissle* and *Hochstein* [8]) even on dynamic measurements, by plotting the reduced complex viscosity $\eta^*(\omega)/B$ over the frequency ω and the reduced shear viscosity $\eta^*(\omega)/B$ over the reduced shear rate $B\dot{\gamma}$, one finds rather good aggreement between $\eta^*(\omega)$ and $\eta(\dot{\gamma})$ in the overlapping frequency range, Fig. 16. The Cox-Merz rule seems to be satisfied. The shift factor B = 3.5 (see also Fig. 12).

3.2.2 Transient Data

3.2.2.1 Shear Flow – Rate Controlled Data

The transient flow behaviour of materials 1P and 2P via imposed rate and imposed stress experiments has been measured at Shell Research and Tech. Center, Louvain la Neuve with cone and plate (radius R = 25 mm; cone angle $\alpha = 0.04$ rad) and parallel plate (radius R = 25 mm; gap of the plates H = –1 mm) rheometers (Rheometrics) at low shear rates and stresses. The steady state viscosities got from these experiments at low shear rate and shear stress conditions seem to obey a power law function (Ostwald-de Waele fluids), Eq. 4, with the consistency K = 842 Pa and the flow exponent n = 0.4 for both samples 1P and 2P, Fig. 17. The aggreement

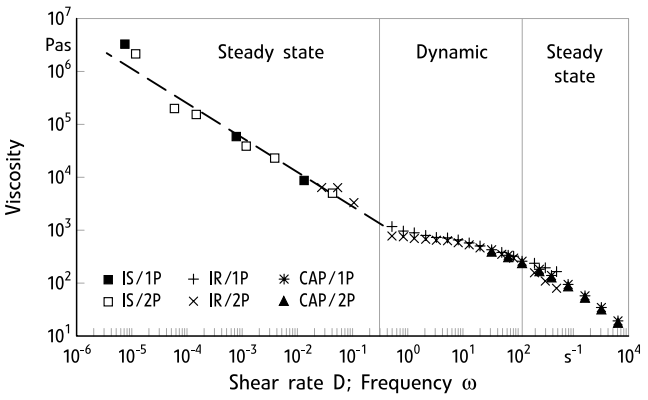

Fig. 17. Flow curves of 1P and 2P. (IS = imposed stress; IR = imposed rate; CAP = capillary measurements)

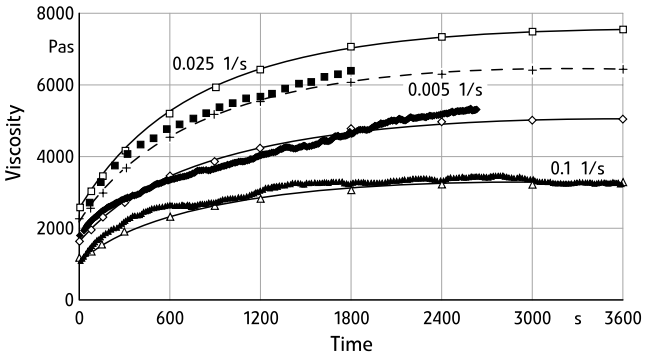

Fig. 18. Viscosity growth data of 2P obtained in a cone and plate geometry at different shear rates compared to model

with dynamic and capillary data (see also Figs. 15 and 16) is acceptable.

$$\eta(t \to \infty) \; = K\dot{\gamma}^{n-1}. \tag{4}$$

Viscosity growth data at different shear rates are given in Fig. 18. Growing from a "starting viscosity" η_a (after short times. The longest relaxation time of the matrix polymer is shorter then 10 s according to the mirror relations; (*Gleissle* [9]). Over long time the steady state viscosity grows to value η.

The transient viscosity $\eta(t)$ can be modeled by an exponential time function, Eq. 5.

$$\eta(t) = \eta_a + (\eta - \eta_a)\,(1 - \exp(-t/\lambda)). \tag{5}$$

It was found, that with a constant time parameter λ (= 770 s) and a constant viscosity ratio η_a/η (= 1.52) the calculated transient viscosity $\eta(t)$ approximates the measured transient viscosity functions with a reasonable accuracy. The steady state viscosities $\eta(t \to \infty)$ were taken from the power law flow function, Eq. 4. Both, calculated and measured data are presented in Fig. 18. The physical background of the long time viscosity growth is not yet known.

3.2.2.2 Shear Flow-Stress Imposed Data

With sample 2P controlled stress experiments had been carried out at $\sigma_{12} = 100$ Pa and 200 Pa. To predict the transient shear deformation Eq. 6 was inversed with respect to the shear deformation with the help of Eq. 5 for $\eta(t)$.

$$\gamma(t) = \int \dot{\gamma}(t)\; dt, \tag{6}$$

$$\dot{\gamma}(t) = \sigma_{12,0}/\eta(t), \tag{7}$$

$$\gamma(t_1) = \int_0^{t_1} [\sigma_{12,0}/\eta(t)]\, dt, \tag{8}$$

$$\gamma(t_1) = \frac{\sigma_{12,0}}{\eta}\lambda\left[\frac{t}{\lambda} + \ln\left(1 - \left(1 + \frac{\eta_a}{\eta}\right)\exp\left(-\frac{t}{\lambda}\right)\right) + \ln\frac{\eta_a}{\eta}\right]. \tag{9}$$

Eq. 9 describes the increase of the shear deformation γ with time in an imposed stress experiment (if $\eta(t)$ is similar to the imposed rate experiment), Fig. 19.

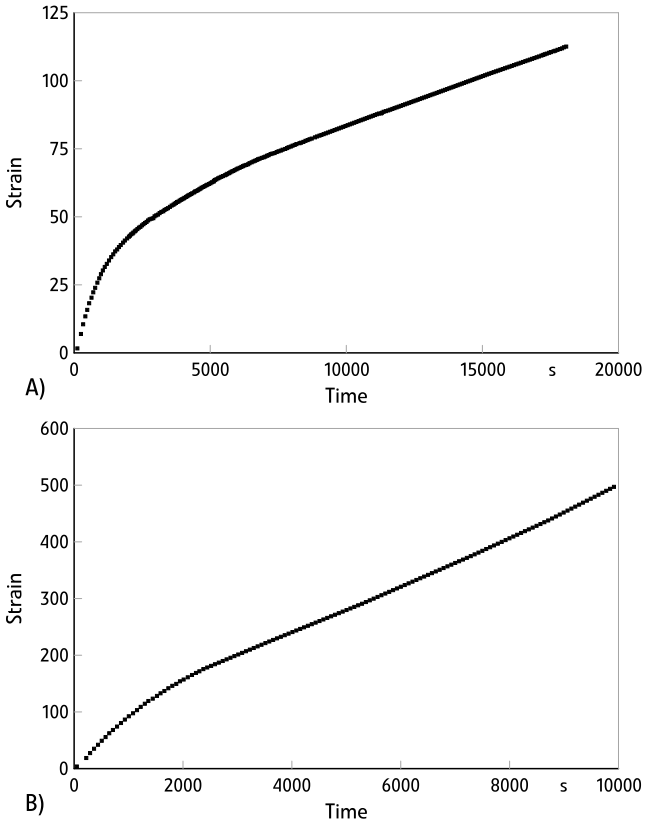

Fig. 19. Shear strain growth of sample 2P in stress controlled shear experiments, A: $\sigma_{12,0}$ = 100 Pa, B: $\sigma_{12,0}$ = 200 Pa

3.2.2.3 Squeeze Flow Experiments

A useful test to study the compression molding process is the sqeeze flow experiment. Circular sample plaques of 25 mm radius and 4 mm height were pressed between polished plates (area 400 · 400 mm) in an Instron material testing machine. In the squeeeze test the height was reduced from 4 mm to 0.9 mm. Each experiment was carried out with two or four plaques pressed simultaniously. The upper plate of the test machine was moved at two different constant speeds (1 and 20 mm/s). The test is a constant volume squeeze test. Assuming no slip at the polished plates and Newtonian flow behaviour one can calculate the apperent shear rate and shear stress at the rim of the plaque from the speed dH/dt and the total force F with the help of the Stefan-equations, Eq. 10 and 11.

$$\dot{\gamma}_{ap,R} = [3(dH/dt)\,(V/\pi)^{1/2}]/[(2H)^{5/2}], \tag{10}$$

$$\sigma_{12,ap,R} = [(2H)^{5/2}F]/[\pi(V/\pi)^{3/2}], \tag{11}$$

where V is the constant volume of the plaque.

Fig. 20 shows the evolution of the force per plaque as a function of the gap height. The force increases nearly linearly in a semi-logarithmic plot meaning that in a constant volume test the flow resistance of the plaque increases logarithmicaly with the gap thickness reduction. At low forces high data scattering was observed. The force for the higher displacement speed is almost one decade higher than for the lower speed.

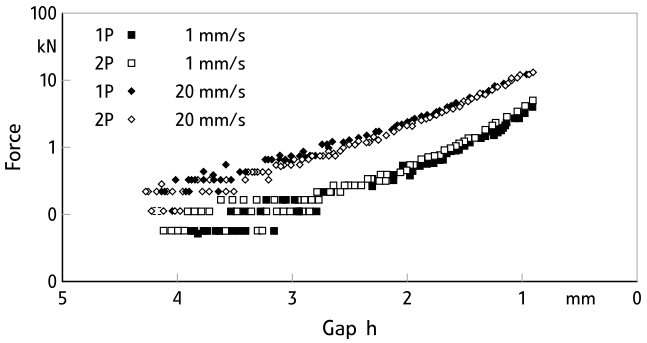

Fig. 20. Force versus displacement for samples 1P and 2P

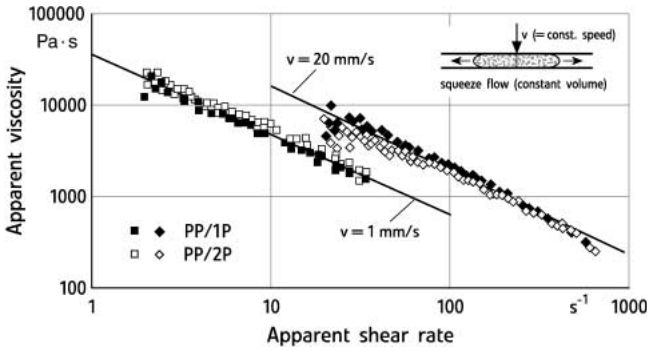

Fig. 21. Apparent squeeze viscosity versus apparent rim shear rate for samples 1P and 2P

Apparent rim viscosity $\eta_{ap,R}$ are calculated with Eqs. 10 and 11 and plotted over the apperent shear rate $\dot{\gamma}_{ap,R}$, Fig. 21. At both speeds a relatively linear relationship is obtained which can be approached by a power law equation (Eq. 12):

$$\sigma_{12,ap,R} = K\dot{\gamma}^{n}_{ap,R}. \quad (12)$$

The power law coefficients, given in Table 4 indicate that the decrease of the squeeze viscosity with increasing shear rate is nearely independent of the squeezing speed (the flow exponents n are close to each other), but at the same shear rate the viscosity calculated from the high shear rate experiment is much higher than for the low speed experiment (see also value of the consistency in Table 4). For the interpretation of this result one should consider that the same apparent shear rate is reached in each plaque at different states of deformation and flow time. The range of overlapping shear rates (20 to 40 s^{-1}) is reached at the very beginning of the deformation at the high speed experiment and at the end of the experiment for the lower speed. A direct comparison is in any case problematic. Comparing the squeeze viscosity measured at Solvay, Brussels, made with constant squeezing velocity, one finds that the viscosity function is about one decade higher than the squeeze viscosity measured at BASF, Ludwigshafen, Germany, with constant load and with constant radius of the squeezed sample.

Speed mm s^{-1}	K Pa	n
1	34 107	0.14
20	123 829	0.10

Table 4. Coefficients of the power law functions (squeeze flow)

4 Optical Observations

4.1 Fibre Orientation in Capillary Flow – Die Entry Observations

To determine the fibre orintation near the orifice of the rheometer capillary, the flow was interrupted and the material was frozen in steady state conditions. The overall convergence picture is shown in Fig. 22.

There are a number of key differences between the virgin (see *Bailey* and *Groves* [3] and Figs. 5, 6, and 7) and the reprocessed material shown here:

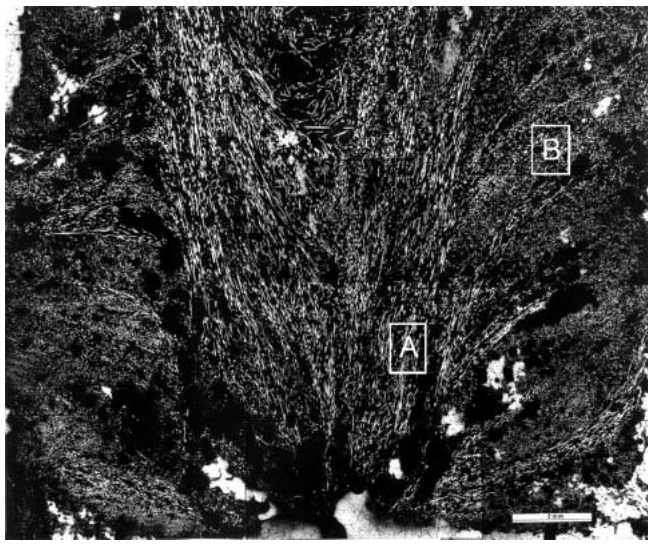

Fig. 22. Processed PP-glass composite (2P) in the convergence zone of a capillary rheometer. The lighter coloured glass fibres are shown against the darker polypropylene background

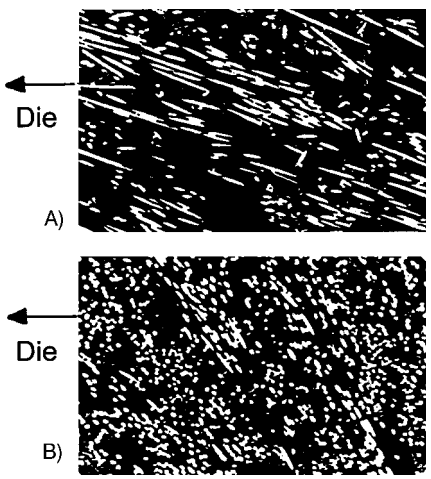

Fig. 23. Optical micrographs: (A) streamlined flow, (B) recirculation zone (both micrographs are 120 magnification and show the die discharge position to the left hand side of the page)

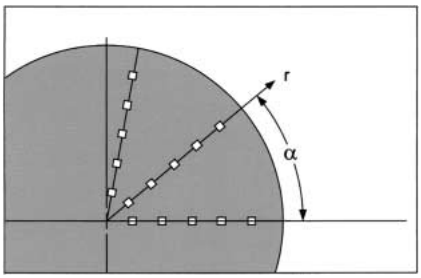

Fig. 24. Position of SEM pictures for the fibre orientation measurements

a) the fibres are less ordered than for the PP/g10 material (10 mm fibres- > 0.6 mm fibre length);
b) the fibres tend to flow in seperate entities (rather than in bundles);
c) fibre rearrangement is clearly easier in the shorter fibre system, and this is reflected in the recirculation zone which shows a variety of fibre alignments;
d) the streamlined flow into the die is quite different. The 10 mm fibres are all alligned well ahead the die whereas the shorter fibres enter the die after coming through a parabolic orientation zone;
e) the die entry cone for the reprocessed material is much shorter than for the pultruded material (10 mm vs 30 mm upstream of the die entry).

The fibre orientations were measured (ICI, Wilton, UK) from a polished section taken through the exact center of the cylinder of frozen material just above the die (The measurements are made on a Kontron image analyser which was used to measure the ellipses produced from the polished section intersecting the fibres.) Two fields of view were studied in each region, the streamlined flow region (A in Figs. 22 and 23), and the recirculation zone (B in Figs. 22 and 23).

A comparison with orientation angle measurements of the feedstock material show that for the shorter fibres of the reprocessed material, the streamlined flow is less aligned while the recirculation zone is less misaligned. These results indicate a significant difference in flow behaviour when the fibres are shorter. Similar observations were made from *Crowson* et al. [10].

4.2 Fibre Orientation in Torsional Flow

In a torsional flow between parallel plates samples of 1P and 2P had been sheared for 20 min with a rim shear rate $\dot{\gamma} = 0.025\ s^{-1}$. To investigate the fibre orientation, the upper surface of the sample was abraded till one third of the thickness was gone. From the polished and gold coated surface, SEM

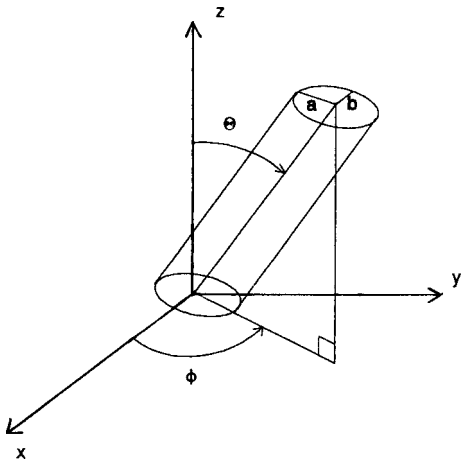

Fig. 26. Definition of angles θ and ϕ; y corresponds to the radial direction

images (Leica stereoscane, magnification 140 times) were taken along 3 radials at 5 different radial positions (1; 6; 11; 16 and 21 mm from the center) as shown in Fig. 24.

A Visilog 4.1.3 image analyser was used to evaluate the fibre orientation. In total 803 fibre sections were identified.

Images taken along a radial direction (constant angle α) at 1; 11; and 21 mm distance from the center are shown in Fig. 25.

From the observations of Fig. 25 it appears that many fibres are already almost in a plane parallel to the plates of the rheometer, because the ellipsoidal cross sections of the fibres have a large aspect ratio (= small to large axis). The picture of the fibres near the center, r = 1 mm seem to be less oriented at first glance. This impression is confirmed in the diagrams of Fig. 27 where the angles θ and ϕ were plotted at the five different radial positions. The result of the three pictures taken at identical radial positions were combined into one to be statistically significant. The definition of the angles θ and ϕ, which are calculated from the amount and direction of the small to large radii of all ellipses can be taken from Fig. 26.

The angles θ were always larger than 60° and are in average between 80 and 90°, which means that the fibre axes of nearly for all fibres, are in the x – y shear plane. These unique orientation can be explaned by the compression of the samples from 2 mm to 1.1 mm height between the plates of the parallel plate rheometer in circumferential direction before the shear experiment. The fibres are preoriented in the shear plane.

The computed angles had values between −90° and +90°. Absolute values of these angles were taken since the interest is primarily on the deviation from radial direction. The distribution of the angles ϕ seem to be random, which can be seen clearly in Fig. 28, where the average values of θ and ϕ, calculated for each radial position r = 1; 6; 11; 16 and 21 mm, are

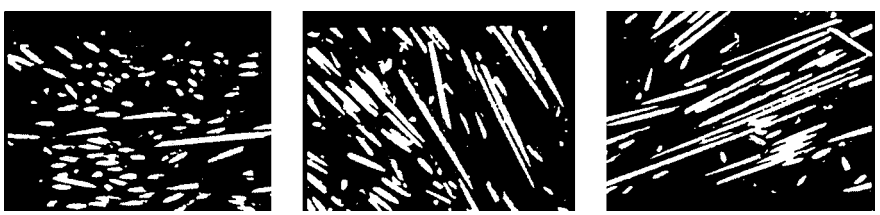

Fig. 25. Typical images of the polished sections at 1 mm (A); 11 mm (B) and 21 mm (C) from the center (vertical direction = radial direction; horizontal = direction of the flow)

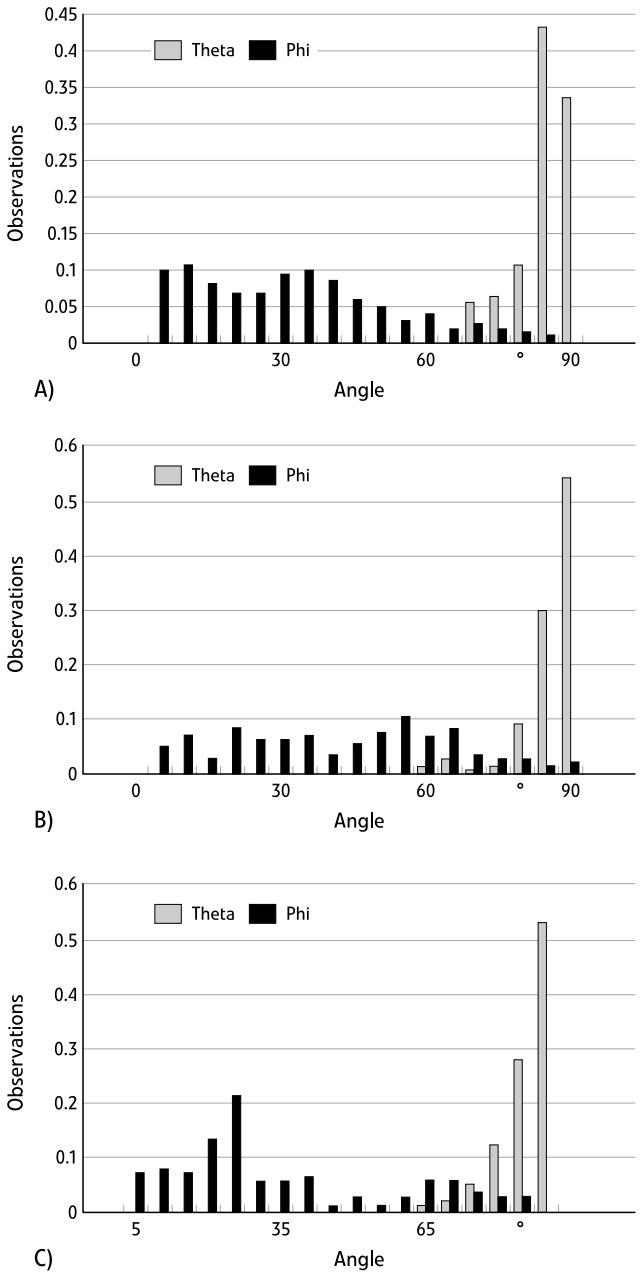

Fig. 27. Frequency plots of angles θ and ϕ at r = 1 mm (A); r = 11 mm (B) and r = 21 mm (C)

shown. The average value of angle ϕ is 45° (independent of the radial position) at the center where we have a small shear deformation as well as near the rim where the shear deformation is twenty times larger. This result can easily be explaned as a consequence of the preorientation of the fibres by the sample preparation. As can be found in Fig. 28 θ is near 90° and hence the fibres are mostly in the x – y shear plane. In a parallel plate flow each element of the x – y plane has the same circumferential velocity (frequency) and hence the fibres will not reorient via the torsional shear flow.

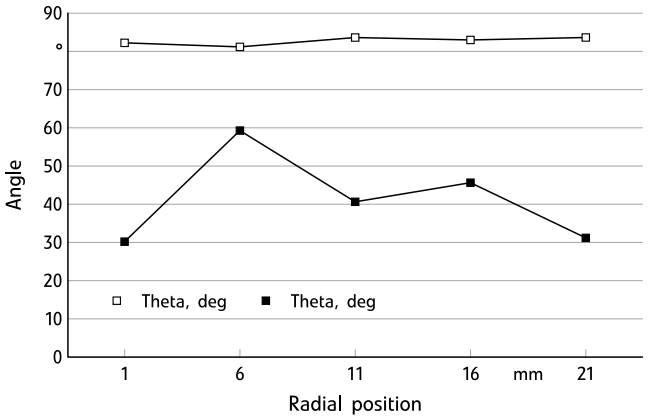

Fig. 28. Evolution of average θ and ϕ values as a function of the radial position

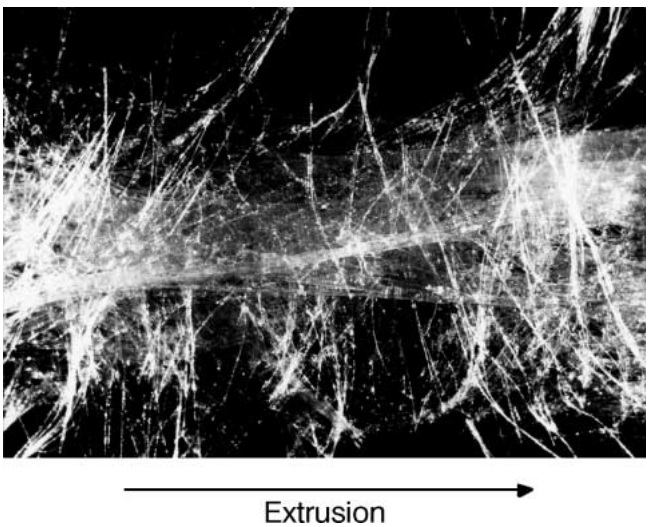

Fig. 29. Verton PP/g10 extruded through a round bore capillary with 2.1 mm diameter

4.3 Shape of the Extrudates

4.3.1 Surface Shape

As was documented: the processing, reprocessing, and testing of the commercial PP-glass composite, Verton, with an initially uniform glass fibre length of 5 or 10 mm influences the structure of the material (fibre length, fibre length distribution, and orientation of the fibres) dramaticaly. As a consequence of the change of structure, the flow behaviour which govern the manufacturing processes and in particular the injection molding process, are changed fundamentaly. This has been shown by quantifying the flow properties.

The deep change of structure and properties can be made immediately obvious by visual observation of capillary extrudates. Fig. 29 gives an impression of the shape (and property) of a strand, extrudated through a round bore capillary with 2.1 mm diameter at rather high extrusion speed. The material is the long fibre compound PP/g10. The extrudate dimension perpindicular to the extrusion direction is more than 10 mm. The extrudate's porosity is near one.

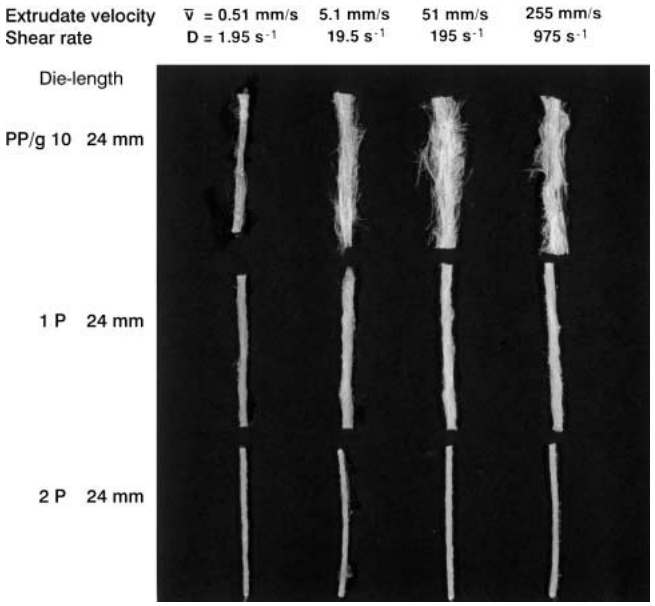

Fig. 30. Compound PP/g10 and reprocessed compounds 1P and 2P extruded at different speeds through a round bore die of 2.1 mm diameter

Fig. 30 demonstrates the change of extrusion properties with first and second reprocessing cycle. While the extrudate shape of of virgin material is, at higher extrusion velocities, nearly independent of the geometry of the die (even slit and round bore dies produce similar extrudate shapes), the shape of extruded reprocessed materials, 1P and 2P, are rather smooth with a crossectional shape similar to the extrusion die.

Fig. 31 shows the same effect of enhanced extrusion properties of reprocessed composites extruded through a slit die.

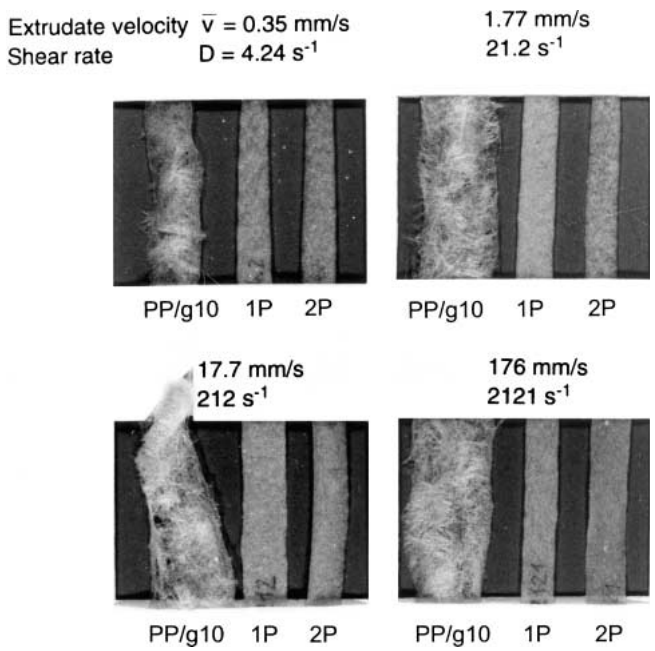

Fig. 31. Compound PP/g10 and reprocessed compounds 1P and 2P extruded through a slit die at different speeds

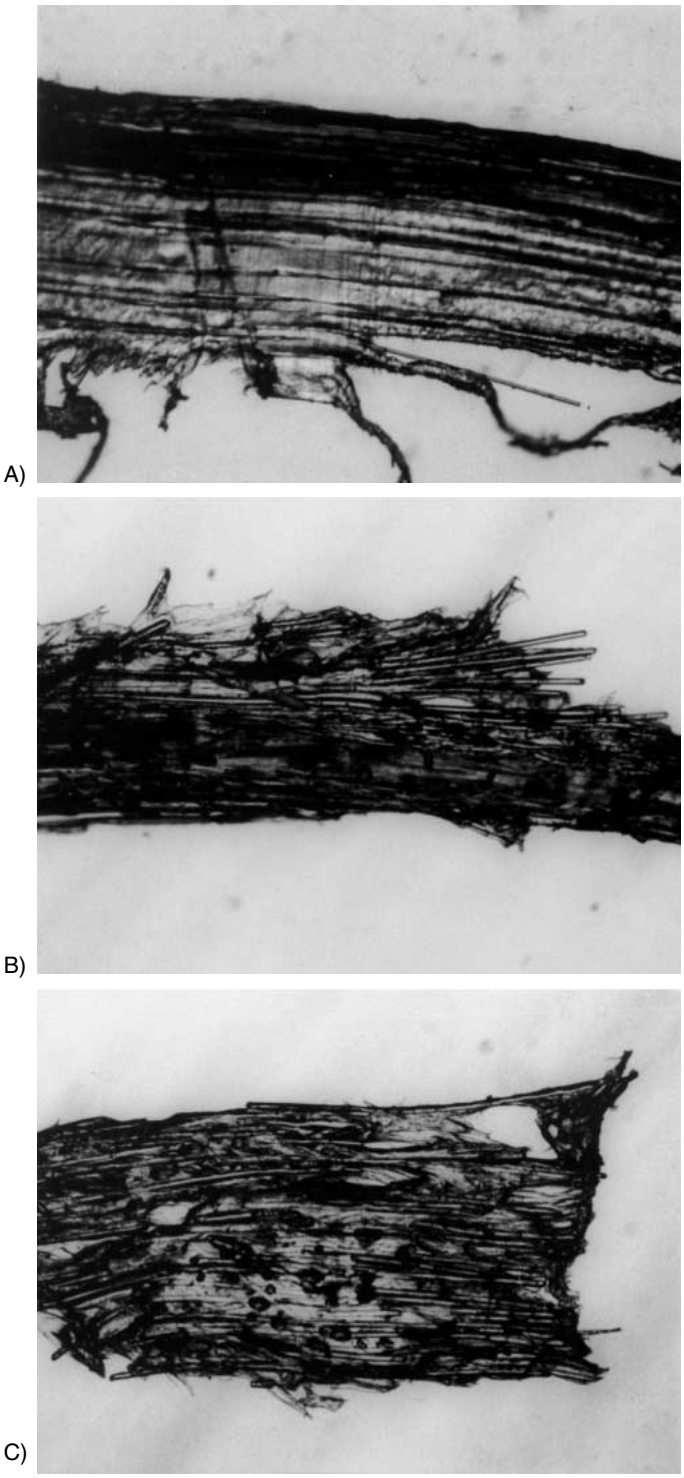

Fig. 32. Strand cut Verton samples PP/g10 (A) and reprocessed samples 1P (B) and 2P (C)

4.3.2 Internal Structure of the Extrudate

The feed stock PP/g10 is a 10 mm pellet with glass fibres aligned on the axis and poorly wetted as can be seen in Fig. 32. With processing, glass fibres are better wetted by the PP-matrix as seen from the photomicrographs of sectioned pellets of 1P and 2P in Fig. 32.

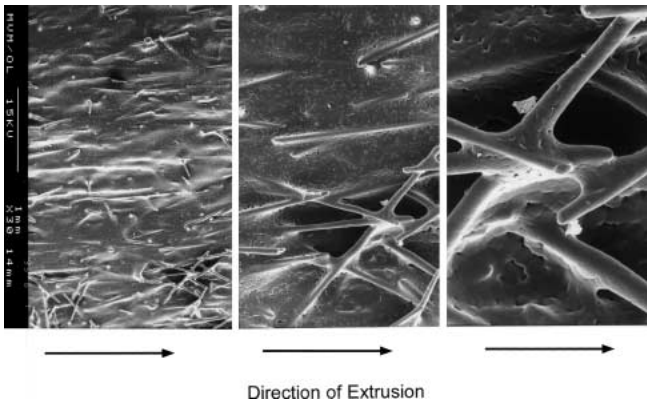

Fig. 33. Sample 1P extruded through a slit die 0.5 · 10 mm with the shear rate D = 2120 s^{-1} and shear stress $\sigma_{12} = 9.21 \cdot 10^4$ Pa

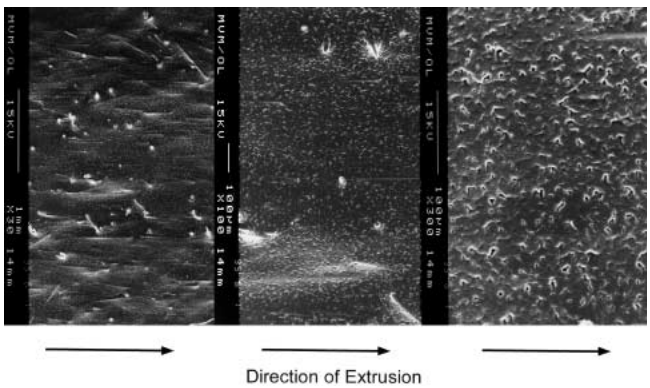

Fig. 34. Sample 2P extruded through slit die 0.5 · 10 mm with shear rate D = 2120 s^{-1} and shear stress $\tau = 8.4 \cdot 10^4$ Pa

SEM-graphs of extruded samples 1P and 2P demonstrate the improved wetting and rather compact output. In Figs. 33 and 34 the surface of strips extruded from a 0.5 · 10 mm slit die at D = 2120 s^{-1} can be seen.

One finds a rather smooth surface with fibres mainly oriented in extrusion direction with few interfacial voids.

The twice reprocessed material, 2P, after a very fast extrusion through the slit die of a capillary rheometer shows a very smooth strip with fibres aligned in flow direction and only small homogeneously dispersed bubbles, Fig. 34.

5 Conclusions

Reprocessing of long fiber composites in plasticating mixers, causes successive fiber length reduction and improved interfacial wetting.

In capillary flow, the fiber length reduction has dramatic effect to reduce entrance pressure losses but the viscous drag within the capillary is generally unaffected. Gleissle's model for reduced flow functions of suspensions with low particle interaction shows that the shear viscosity property of the composite is dominated by and predictable from the matrix resin.

In contrast to the base resin, the composite demonstrates reduced entry pressure drop at lower cone entry angle. Fiber orientations in the entry region are improved at shorter fiber length and lower cone entry angle.

In complex flow, the composites demonstrate non linear behavior at any significant strain and especially at low frequency and without repeated reprocessing. Modified Casson plots indicate lower yield values with repeated reprocessing. Application of reduced flow function to the complex data is validated by the agreement of capillary and complex reduced viscosity in the overlapping shear rate range.

In steady rotation, the composites demonstrate a viscosity growth which is predicted by a first order model. Both stress and strain growth are predictable by inverting model parameters.

The squeeze flow experiment shows increased flow resistance (compressive viscosity) with decreased gap and increased squeeze rate. All viscosity functions: shear flow in capillary, in dynamic parallel test, and in steady parallel test mode, as well as squeeze flow can be approximated by power law functions.

Flow visualization via fiber orientation in frozen sections was performed in capillary and parallel plate apparata. In the capillary, the shorter fiber of reprocessed sample was more easily oriented in the entry zone but was more easily misoriented in the capillary than virgin feed. In torsional tests, the reprocessed composite's fibers were strictly aligned in the radial plane with no preferred circumferential orientation.

High speed capillary or strip extrusion caused progressive interfacial failure in the virgin material while the surface quality and interfacial integrity improved with composite reprocessing.

References

1 *Cervenka, A. J., Allan, P. S.:* Pure & Appl. Chem., 8, p.1693 (1997)
2 *v. Bradsky, G. J., Bailey, R. S., Cervenka, A. J., Zachmann, H. G., Allen, P. S.:* Pure & Appl. Chem., 12, p. 2523 (1997)
3 *Bailey, R. S., Groves, D. J.:* Pure & Appl. Chem., 12, p. 2541 (1997)
4 *Laun, H. M.:* Colloid & Polymer Sci. 262, p. 257 (1984)
5 *Gleissle, W., Baloch, M. K.:* Proceeding of the IX. Int. Congr. on Rheol., Accapulco, Mexico (1984)
6 *Ohl, N., Gleissle, W.:* J. Rheol. 37(2), p. 381 (1993)
7 *Utracki, L. J.:* Polym. Composites 7 p. 274 (1986)
8 *Gleissle, W., Hochstein, B.:* Proceeding of the 4th Eur. Rheol. Conf., p. 648 (1994)
9 *Gleissle, W.:* Proceeding of the VIII Int. Congr. on Rheol., p. 457, Naples (1980)
10 *Crowson, R. J., Folkes, M. J., Bright, P. F.:* Polym. Eng. and Sci. 14, p. 925 (1980)

Date received: October 10, 2002
Date accepted: December 10, 2002